High-spin states in doubly odd ^{162,164}Lu

M. A. Cardona,[1,2] J. Davidson,[3,4] D. Hojman,[1,2,4] M. E. Debray,[1,2] A. J. Kreiner,[1,2,4] H. Somacal,[1,2] M. Davidson,[3,4] D. R. Napoli,[5] D. Bazzacco,[6] N. Blasi,[7] R. Burch,[5] D. De Acuña,[5] S. M. Lenzi,[6] G. Lo Bianco,[7] J. Rico,[5] and C. Rossi Alvarez[6]

[1]*Departamento de Física, Comisión Nacional de Energía Atómica, 1429 Buenos Aires, Argentina*

[2]*Universidad de San Martín, San Martín, Argentina*

[3] *Departamento de Física, Facultad de Ciencias Exactas y Naturales, Universidad de Buenos Aires, Buenos Aires, Argentina*

[4]*CONICET, 1033 Buenos Aires, Argentina*

[5]*INFN, Laboratori Nazionali di Legnaro, Legnaro, Italy*

[6]*Dipartimento di Fisica, Sezione di Padova, Padova, Italy*

[7]*Dipartimento di Fisica and INFN, Sezione di Milano, Milano, Italy*

(Received 4 February 1997)

High-spin states in ^{162}Lu and ^{164}Lu have been studied by means of in-beam γ-ray spectroscopy techniques using the multidetector array GASP. The excited states have been populated through the ^{139}La(^{28}Si,5n)^{162}Lu and ^{139}La[$^{29(30)}$Si,4(5)n]^{164}Lu reactions. Level schemes were constructed for both nuclei. Configurations for the rotational bands have been discussed. Alignments, band crossing frequencies, and $B(M1)/B(E2)$ ratios have been analyzed in the framework of the cranking model. The systematic evolution of the signature inversion in the $\pi h_{11/2}\otimes \nu i_{13/2}$ structure is reviewed. [S0556-2813(97)00208-2]

PACS number(s): 21.60.Ev, 21.60.Fw, 23.20.Lv, 27.70.+q

I. INTRODUCTION

The present work extends the systematic investigation of doubly odd Lu nuclei to lighter isotopes. Recently a series of studies have been started on doubly odd Lu isotopes (^{166}Lu [1], ^{168}Lu [2], ^{170}Lu [3], ^{172}Lu [4], and ^{174}Lu [5]) and here we present spectroscopic investigations of the rotational structures in ^{162}Lu and ^{164}Lu. Doubly odd nuclei are unique candidates to study proton-neutron coupling schemes, proton-neutron interactions, and for the investigation of phenomena such as the delay in the band crossing frequency due to the possibility of performing double-blocking experiments [6]. Another remarkable effect that has been observed in odd-odd nuclei is signature inversion [7,8]. The occurrence of this phenomenon has been found in bands of high j parentage throughout the chart of nuclides, for example in the Br-Rb region [7] concerning the $\pi g_{9/2}\otimes \nu g_{9/2}$ structure and in the $A\approx 130$ mass region involving the $\pi h_{11/2}\otimes \nu h_{11/2}$ structure [9]. Another observation of signature inversion concerns the $\pi h_{11/2}\otimes \nu i_{13/2}$ structure which corresponds to the yrast band in nuclei of the light rare-earth region (Eu, Tb, Ho, Tm [10,11]).

Prior to the beginning of this work the information about ^{162}Lu and ^{164}Lu was comprised of the ground state and some excited states populated through the ^{162}Hf and ^{164}Hf decay, respectively [12,13]. Some of the results presented here have been reported earlier [14]. During the course of the present investigation some results about in beam studies became available for ^{162}Lu [15,16] and ^{164}Lu [17,18].

II. EXPERIMENTS AND RESULTS

A. Measurements in ^{162}Lu

High-spin states of ^{162}Lu were populated through the ^{139}La(^{28}Si,5n) reaction at 160 MeV. The target consisted of a 1 mg/cm^2 La, gold backed (4 mg/cm^2) foil, protected by a 30 μg/cm^2 gold layer on the front side. The beam was provided by the Tandem XTU accelerator of Legnaro and γ rays emitted by the reaction residues were detected using the GASP array [20], which consisted, for this coincidence experiment, of 39 Compton suppressed large volume Ge detectors, a planar detector, and a multiplicity filter of 80 BGO elements. Events were collected when at least three suppressed Ge and three inner multiplicity filter detectors were fired. With this condition the event rate was around 4–5 kHz and a total of 2.7×10^8 events were recorded. The assignment of γ rays to ^{162}Lu was based on coincidences with Lu K x rays, previous knowledge of the neighboring Lu isotopes (^{161}Lu [21] and ^{163}Lu [22]), and multiplicity distributions.

A matrix of γ-ray energy in the Ge detectors vs BGO multiplicity was useful to find assignments of γ transitions to different reaction products. To select only neutron channels, leading to Lu isotopes, the matrix E_γ vs BGO multiplicity was constructed with a gate condition on Lu K x rays, suppressing in this way reaction channels involving the evaporation of charged particles such as one proton leading to Yb isotopes and one α particle leading to Tm isotopes, which have a non-negligible contribution to the total cross section. Three cuts of this matrix are shown in Fig. 1, giving a clear indication of the changes in the γ spectrum resulting from different multiplicity conditions; lines belonging to ^{161}Lu ($6n$ channel) and ^{163}Lu (4n channel) isotopes are strong for low and high multiplicity, respectively. Figure 2 shows the BGO multiplicity distribution of the different neutron channels obtained by gating on pure transitions belonging to ^{161}Lu and ^{163}Lu and on the 299.9 keV line assigned to ^{162}Lu, with the additional gate condition on the Lu K x ray. All the γ rays assigned to ^{162}Lu were those with the multiplicity distribution corresponding to a five-particle channel.

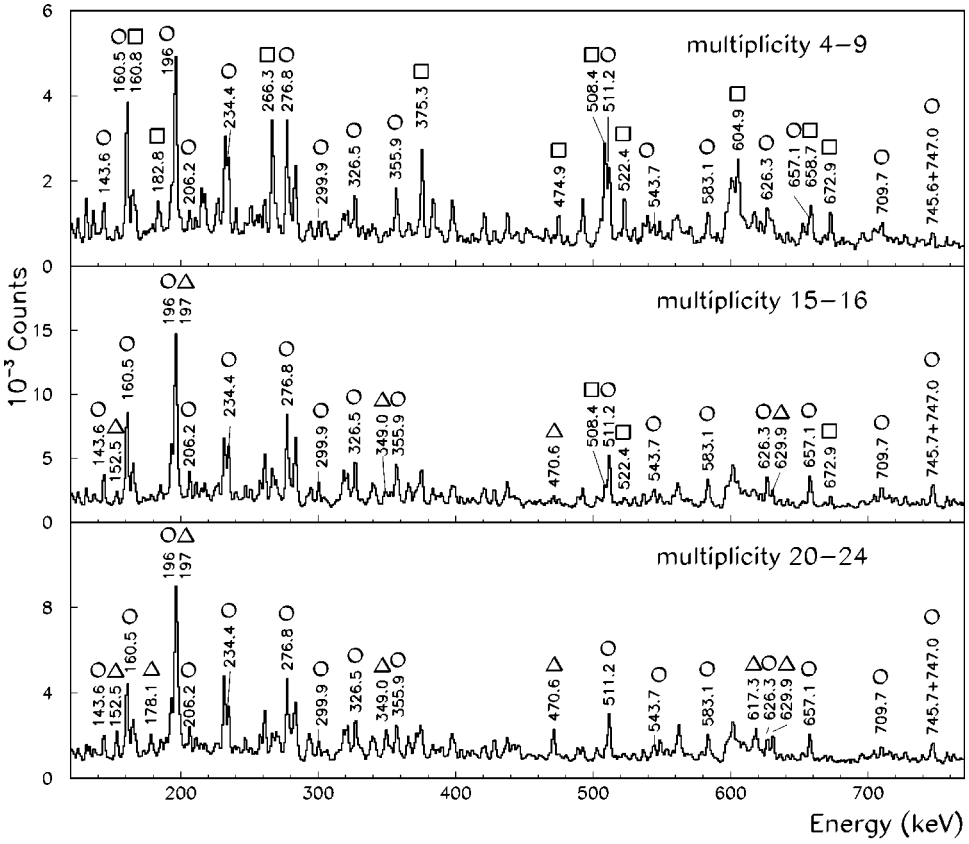

FIG. 1. Projected γ-ray spectra with BGO filter multiplicity conditions and gated on Lu K x rays for the reaction ^{139}La + ^{28}Si at 160 MeV. The most important and clean lines belonging to Lu isotopes are indicated: squares for ^{161}Lu, circles for ^{162}Lu, and triangles for ^{163}Lu.

B. Measurements in ^{164}Lu

High-spin states of the doubly odd nucleus ^{164}Lu have been populated through fusion-evaporation reactions. In order to determine the optimum energy to run a coincidence experiment at Legnaro excitation functions were obtained through the ^{139}La(^{29}Si,4n) reaction in the energy range $E(^{29}\mathrm{Si}) = 135-150$ MeV at the TANDAR accelerator in Buenos Aires. The γ-ray coincidence experiment was performed subsequently at the Legnaro Tandem Facility using the 4π array GASP [20] consisting, for this experiment, of 35 Compton suppressed Ge's (80% efficiency), two planar detectors, in order to be sensitive to low γ-ray energies, and 80 BGO detectors, providing the sum-energy and γ-ray multiplicity used to select the different reaction channels. Triple events (more than three Ge counters fired) with more than three hits in the inner multiplicity filter, were taken at about 8 kHz for the reactions ^{139}La(^{29}Si,4n) and ^{139}La(^{30}Si,5n) at 145 and 157 MeV bombarding energy, respectively. A total of 1.6×10^{8} and 6×10^{7} threefold or higher coincidence events were recorded during the experiment bombarding with ^{29}Si and ^{30}Si, respectively. The target consisted of a 1 mg/cm^2 La, gold backed (4 mg/cm^2) foil. The isotopic identification was based on coincidences with Lu K x rays, previous knowledge of the neighboring Lu isotopes (^{163}Lu [22], ^{165}Lu [23,24]), and multiplicity distributions. Figure 3 shows projected planar γ-ray spectra for the reactions induced by the two projectiles (^{29}Si and ^{30}Si). In the spectra [Figs. 3(a) and 3(b)] the most important lines belonging to the known reaction channels ^{163}Lu, ^{165}Lu, and ^{164}Yb [25] have been indicated together with the lines assigned to ^{164}Lu (93.1, 140.9, 162.1, 165.5, 237.0 keV, etc.). Further confirmation of this assignment was made through the study of the BGO multiplicity spectra of strong γ rays. Figures 4(a) and (b) show the BGO multiplicity spectra of the different reaction channels obtained by gating on selected strong uncontaminated lines belonging to the neighboring known ^{163,165}Lu isotopes and on the 237.0 keV line. From Fig. 4 it can be seen that the 237.0 keV transition, assigned to ^{164}Lu, shows the correct fold corresponding to a four-particle and five-particle channel for the reactions with ^{29}Si and ^{30}Si projectiles, respectively.

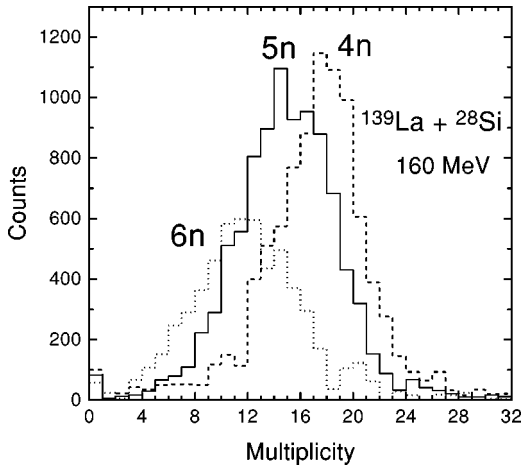

FIG. 2. Multiplicity distribution of neutron channels in the reaction ^{139}La + ^{28}Si at 160 MeV, obtained by gating on strong and clean lines: 4n, 470.6 keV belonging to ^{163}Lu, 5n, 299.9 keV assigned to ^{162}Lu, and 6n, 474.9 keV belonging to ^{161}Lu. These distributions have additional gate condition on Lu K x rays.

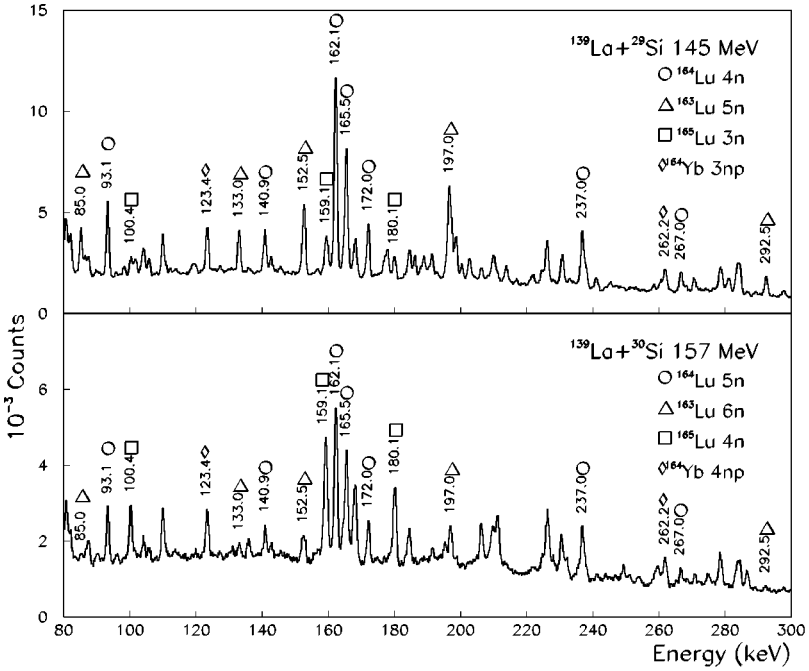

FIG. 3. Projected γ spectra of planar detectors for the two reactions ^{139}La + ^{29}Si at 145 MeV and ^{139}La + ^{30}Si at 157 MeV. The transitions assigned to ^{164}Lu are indicated with a circle.

C. Level scheme of ^{162}Lu

The level scheme for ^{162}Lu deduced from the data obtained here is shown in Fig. 5. Figure 6 shows summed coincidence spectra gated on pairs of transitions belonging to a given band. The 97.8 keV γ ray was proposed to belong to band A by both coincidence evidence and systematics, but the uncertainty in the presence of the 293.4 keV crossover transition, due to low intensity and contaminations, made it difficult to confirm its placement. The yrast band (band A), decays through several transitions, some of which are shown in Fig. 6(a): 80.6, 108.2, 143.6, 164.4, 266.0, and 269.0 keV. These lines could not be placed unambiguosly into the level scheme, however, from their coincidence relationships an excitation energy greater than 400 keV was estimated for the (10^-) state of the yrast band. Band B decays to band A through the 681.8, 788.4, and 908.2 keV transitions. For the strongest one, the 788.4 keV line, the measured DCO ratio 0.54 ± 0.14 is consistent with a stretched dipole for our geometry. In the neighboring ^{161,163}Lu isotopes [21,22], stretched dipole transitions with similar energy values have been observed connecting side bands with the yrast bands.

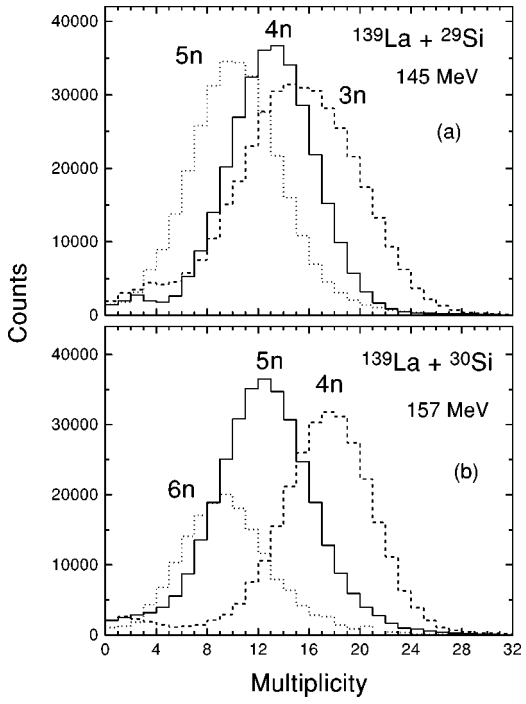

FIG. 4. Multiplicity distribution of neutron channels (a) in the reaction ^{139}La + ^{29}Si at 145 MeV, obtained by gating on the strong lines $3n$, 159.1 keV belonging to ^{165}Lu, $4n$, 237.0 keV assigned to ^{164}Lu, and $5n$, 470.6 keV belonging to ^{163}Lu. (b) for the reaction ^{139}La + ^{30}Si at 157 MeV, gating on the strong lines $4n$, 180.1 keV belonging to ^{165}Lu, $5n$, 237.0 keV assigned to ^{164}Lu, and $6n$, 197 keV belonging to ^{163}Lu.

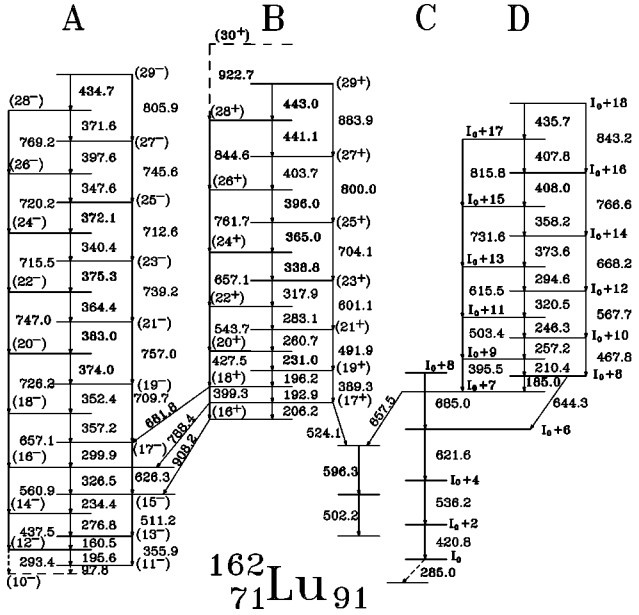

FIG. 5. Level scheme of ^{162}Lu proposed in the present work.

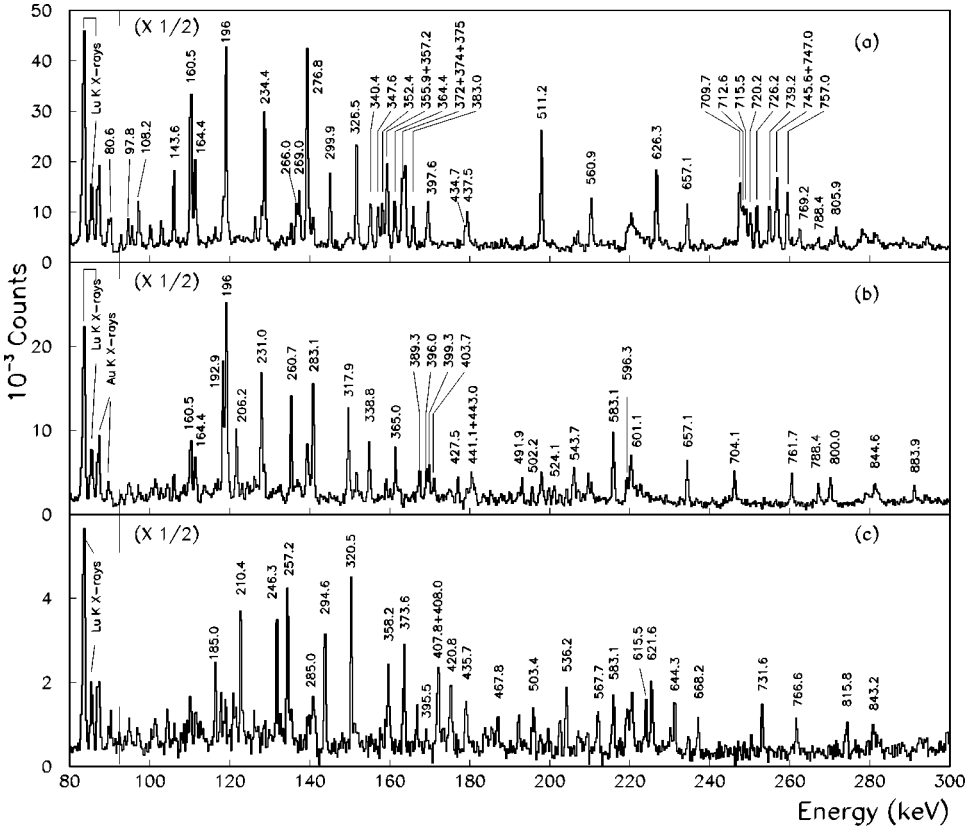

FIG. 6. γ ray coincidence spectra corresponding to the sum of several gates on pairs of transitions belonging to band A (a), band B (b), and band D (c) of ^{162}Lu.

From this analogy, the 788.4 keV transition was assumed to be a stretched $E1$, allowing the spin and parity of band B to be fixed relative to band A. At spin greater than $20\hbar$ band B becomes yrast. The 583.1 keV line indicated in Figs. 6(b) and 6(c) in strong coincidence with members of band B and D, depopulates these bands in a way which was not possible to establish. Band D feeds a quadrupole cascade of γ rays, 420.8, 536.2, 621.6, and 644.3 keV (labeled in Fig. 5 as band C). Lines belonging to bands C and D are indicated in Fig. 6(c). Transition energies, spin assignments, γ intensities, branching ratios, DCO ratios, and $B(M1)/B(E2)$ ratios in ^{162}Lu are listed in Table I grouped in sequences for each band.

D. Level scheme of ^{164}Lu

The level scheme of ^{164}Lu obtained from the present work is shown in Fig. 7. Summed coincidence spectra obtained by setting gates on transitions belonging to bands A, B, and C are shown in Figs. 8(a), 8(b), and 8(c), respectively. For bands A and C double gated spectra have been added. Figure 8(d) shows a γ-ray coincidence spectrum obtained with a gate on the 401.2 keV transition belonging to band D. The yrast sequence indicated in Fig. 7 as band A is depopulated by several transitions, which could not be placed in the level scheme. Some of the strongest lines are indicated in Fig. 8(a): 143.0, 171.5, and 184.9 keV. The 162.1 keV transition is an unresolved doublet; one component has been placed in band A, while the other one depopulates the same band A. Band B is connected to band C by the 647.8 and the 252.0 keV γ rays. The DCO ratio for the 647.8 keV line (1.1 ± 0.2) is consistent with a stretched quadrupole transition. Further connections between bands B and C are likely, but could not be established because of intensity limitations and contamination of the linking lines. The 647.8 keV line fixes the relative energy between bands B and C as well as spins and parities. From the spin assignments the two (19^+) states in band B and C lie very close to each other (14 keV of energy difference) and it is expected that their wave functions are largely admixed, favoring at this point the linkage between the bands. Band B depopulates into the yrast band through the 864.9 and 964.6 keV transitions both of which have stretched dipole nature deduced from DCO ratios (see Table II). Based on the same arguments discussed above for the 788.4 keV line in ^{162}Lu, $E1$ character was adopted for the 864.9 and 964.6 keV transitions.

The energies, spin assignments, intensities, and DCO ratios for γ rays assigned to ^{164}Lu are listed in Table II, grouped in sequences for each band. In both cases ^{162}Lu and ^{164}Lu γ-ray intensities were obtained from the total coincidence projections and from individual spectra in coincidence with low spin transitions. The γ-ray intensities in Table II were extracted from the ^{139}La(^{29}Si,$4n$) reaction at 145 MeV.

The DCO γ-γ matrices were created sorting on one axis the detectors lying at $\theta_1 \approx 34°$, 36°, 144°, and 146° and on the other those at $\theta_2 = 90°$ with respect to the beam direction. In the GASP geometry, setting gates on stretched quadrupole transitions, the theoretical DCO ratios $I\gamma_{\text{gate}=\theta_2}(\theta_1)/I\gamma_{\text{gate}=\theta_1}(\theta_2)$ are ≈ 1 for stretched quadrupole transitions and ≈ 0.5 for pure dipole ones.

The experimental branching ratios for a given state listed in Tables I and II were obtained from relative γ-ray intensities in the spectrum in coincidence with transitions directly populating that state, except for some of the higher levels, where the ratio of the intensities listed in the third column of

TABLE I. γ-ray transition energies, spin assignments, γ intensities, branching ratios, DCO ratios, and $B(M1)/B(E2)$ ratios in ^{162}Lu.

E_γ (keV) [a]	$I_i^\pi \rightarrow I_f^\pi$ [b]	I_γ [c]	Branching ratio [d]	DCO ratio [e]	$B(M1)/B(E2)$ [f] (μ_N^2/e^2b^2)
Band A					
97.8	$(11^-)\rightarrow(10^-)$	95			
195.6	$(12^-)\rightarrow(11^-)$	1000		0.70±0.14	
293.4	$(12^-)\rightarrow(10^-)$				
160.5	$(13^-)\rightarrow(12^-)$	650	0.45±0.05	0.77±0.12	2.1±0.2
355.9	$(13^-)\rightarrow(11^-)$	340		1.3±0.4	
276.8	$(14^-)\rightarrow(13^-)$	729	0.50±0.06	0.77±0.09	1.05±0.13
437.5	$(14^-)\rightarrow(12^-)$	310		1.2±0.2	
234.4	$(15^-)\rightarrow(14^-)$	416	1.25±0.13	0.69±0.10	1.50±0.15
511.2	$(15^-)\rightarrow(13^-)$	586		0.95±0.14	
326.5	$(16^-)\rightarrow(15^-)$	406	0.84±0.15	0.78±0.12	1.3±0.2
560.9	$(16^-)\rightarrow(14^-)$	345		0.95±0.25	
299.9	$(17^-)\rightarrow(16^-)$	173	1.85±0.15	0.73±0.15	1.34±0.11
626.3	$(17^-)\rightarrow(15^-)$	277		0.98±0.14	
357.2	$(18^-)\rightarrow(17^-)$	186	1.7±0.3	0.73±0.21	1.1±0.2
657.1	$(18^-)\rightarrow(16^-)$	313		1.2±0.2	
352.4	$(19^-)\rightarrow(18^-)$	130	2.2±0.4	0.80±0.20	1.3±0.2
709.7	$(19^-)\rightarrow(17^-)$	240		0.83±0.25	
374.0	$(20^-)\rightarrow(19^-)$	113	1.7±0.3		1.6±0.3
726.2	$(20^-)\rightarrow(18^-)$	192		0.81±0.12	
383.0	$(21^-)\rightarrow(20^-)$	77	2.2±0.4	0.76±0.16	1.4±0.2
757.0	$(21^-)\rightarrow(19^-)$	152		0.92±0.18	
364.4	$(22^-)\rightarrow(21^-)$	75	2.4±0.6		1.4±0.4
747.0	$(22^-)\rightarrow(20^-)$	180			
375.3	$(23^-)\rightarrow(22^-)$	66	1.9±0.5		1.5±0.4
739.2	$(23^-)\rightarrow(21^-)$	110		1.05±0.16	
340.4	$(24^-)\rightarrow(23^-)$	90	1.5±0.3	0.68±0.23	2.2±0.4
715.5	$(24^-)\rightarrow(22^-)$	140		1.0±0.3	
372.1	$(25^-)\rightarrow(24^-)$	70	1.4±0.4		1.8±0.5
712.6	$(25^-)\rightarrow(23^-)$	113		1.4±0.4	
347.6	$(26^-)\rightarrow(25^-)$	90	1.4±0.3		2.3±0.5
720.2	$(26^-)\rightarrow(24^-)$	130		1.0±0.2	
397.6	$(27^-)\rightarrow(26^-)$	65	1.1±0.4	0.67±0.13	1.9±0.7
745.6	$(27^-)\rightarrow(25^-)$	74			
371.6	$(28^-)\rightarrow(27^-)$	45	1.3±0.4		2.8±0.9
769.2	$(28^-)\rightarrow(26^-)$	67			
434.7	$(29^-)\rightarrow(28^-)$	42	1.4±0.5		2.1±0.7
805.9	$(29^+)\rightarrow(27^-)$	62			
Band B					
206.2	$(17^+)\rightarrow(16^+)$	197		0.85±0.17	
192.9	$(18^+)\rightarrow(17^+)$	380	0.42±0.04	0.80±0.15	2.3±0.2
399.3	$(18^+)\rightarrow(16^+)$	142			
196.2	$(19^+)\rightarrow(18^+)$	287	0.50±0.10		1.6±0.3
389.3	$(19^+)\rightarrow(17^+)$	143			
231.0	$(20^+)\rightarrow(19^+)$	253	0.42±0.08	0.86±0.20	1.9±0.3
427.5	$(20^+)\rightarrow(18^+)$	110		1.3±0.3	
260.7	$(21^+)\rightarrow(20^+)$	210	0.59±0.09	0.48±0.12	2.3±0.3
491.9	$(21^+)\rightarrow(19^+)$	106			
283.1	$(22^+)\rightarrow(21^+)$	234	0.77±0.14	0.80±0.14	1.9±0.3
543.7	$(22^+)\rightarrow(20^+)$	131			
317.9	$(23^+)\rightarrow(22^+)$	145	0.83±0.13	0.70±0.20	2.0±0.3
601.1	$(23^+)\rightarrow(21^+)$	143			
338.8	$(24^+)\rightarrow(23^+)$	106	0.91±0.18	0.70±0.14	2.4±0.5
657.1	$(24^+)\rightarrow(22^+)$	128			
365.0	$(25^+)\rightarrow(23^+)$	92	1.1±0.2		2.2±0.4
704.1	$(25^+)\rightarrow(24^+)$	125			
396.0	$(26^+)\rightarrow(25^+)$	83	1.0±0.3		2.9±0.9
761.7	$(26^+)\rightarrow(24^+)$	85			
403.7	$(27^+)\rightarrow(26^+)$	49	2.9±0.5		1.2±0.2
800.0	$(27^+)\rightarrow(25^+)$	100			
441.1	$(28^+)\rightarrow(27^+)$	46			
844.6	$(28^+)\rightarrow(26^+)$				
443.0	$(29^+)\rightarrow(28^+)$	33	1.5±0.4		2.9±0.8

TABLE I. (*Continued*).

E_γ (keV) [a]	$I_i^\pi \rightarrow I_f^\pi$ [b]	I_γ [c]	Branching ratio [d]	DCO ratio [e]	$B(M1)/B(E2)$ [f] (μ_N^2/e^2b^2)
883.9	$(29^+)\rightarrow(27^+)$	48			
922.7	$(30^+)\rightarrow(28^+)$	48			
Transitions between A and B					
681.8	$(18^+)\rightarrow(17^-)$	31			
788.4	$(17^+)\rightarrow(16^-)$	132		0.54±0.14	
908.2	$(16^+)\rightarrow(15^-)$	39			
Band C					
420.8	$I_0+2\rightarrow I_0$	126		1.3±0.3	
536.2	$I_0+4\rightarrow I_0+2$	104		1.0±0.2	
621.6	$I_0+6\rightarrow I_0+4$	88		0.9±0.2	
685.0	$I_0+8\rightarrow I_0+6$	32			
Band D					
185.0	$I_0+8\rightarrow I_0+7$	32			
210.4	$I_0+9\rightarrow I_0+8$	113	0.33±0.07	0.63±0.20	2.2±0.5
395.5	$I_0+9\rightarrow I_0+7$	40			
257.2	$I_0+10\rightarrow I_0+9$	104	0.29±0.03	0.68±020	3.2±0.3
467.8	$I_0+10\rightarrow I_0+8$	61			
246.3	$I_0+11\rightarrow I_0+10$	97	0.56±0.11	0.35±0.17	2.7±0.5
503.4	$I_0+11\rightarrow I_0+9$	51			
320.5	$I_0+12\rightarrow I_0+11$	94	0.59±0.13		2.1±0.5
567.7	$I_0+12\rightarrow I_0+10$	46			
294.6	$I_0+13\rightarrow I_0+12$	82	0.65±0.15	0.56±0.22	3.7±0.9
615.5	$I_0+13\rightarrow I_0+11$	63			
373.6	$I_0+14\rightarrow I_0+13$	45	0.8±0.2		2.2±0.5
668.2	$I_0+14\rightarrow I_0+12$	41			
358.2	$I_0+15\rightarrow I_0+14$	35	1.1±0.2		2.9±0.5
731.6	$I_0+15\rightarrow I_0+13$	41			
408.0	$I_0+16\rightarrow I_0+15$	30	1.3±0.3		2.1±0.5
766.6	$I_0+16\rightarrow I_0+14$	38			
407.8	$I_0+17\rightarrow I_0+16$	26	1.4±0.3		2.6±0.6
815.8	$I_0+17\rightarrow I_0+15$	36			
435.7	$I_0+18\rightarrow I_0+17$				
843.2	$I_0+18\rightarrow I_0+16$	31			
Transitions between C and D					
644.3	$I_0+18\rightarrow I_0+16$	41		0.9±0.3	
Other transitions					
285.0					
502.2		90			
524.1		38			
583.1 [g]		404			
596.3		88			
657.5		42			

[a]Uncertainties between 0.1 and 0.3 keV.
[b]Spin assignment based on systematics.
[c]Uncertainties between 5 and 30 %.
[d]Branching ratio: $I\gamma(I\rightarrow I-2)/I\gamma(I\rightarrow I-1)$, $I\gamma(I\rightarrow I-2)$ and $I\gamma(I\rightarrow I-1)$ are the relative γ intensities of the quadrupole and dipole transition depopulating the spin I level, respectively.
[e]Directional correlation ratio: $I\gamma_{\text{gate}=\theta_2}(\theta_1)/I\gamma_{\text{gate}=\theta_1}(\theta_2)$, ($\theta_1\approx 32°$, 36°, 144°, and 148° and $\theta_2=90°$) determined from coincidence spectra, setting gates on stretched $E2$ transitions on both axes of the DCO matrix.
[f]Determined assuming $\delta^2=0$.
[g]583.1 keV transition, not placed in the level scheme, depopulates bands B and D.

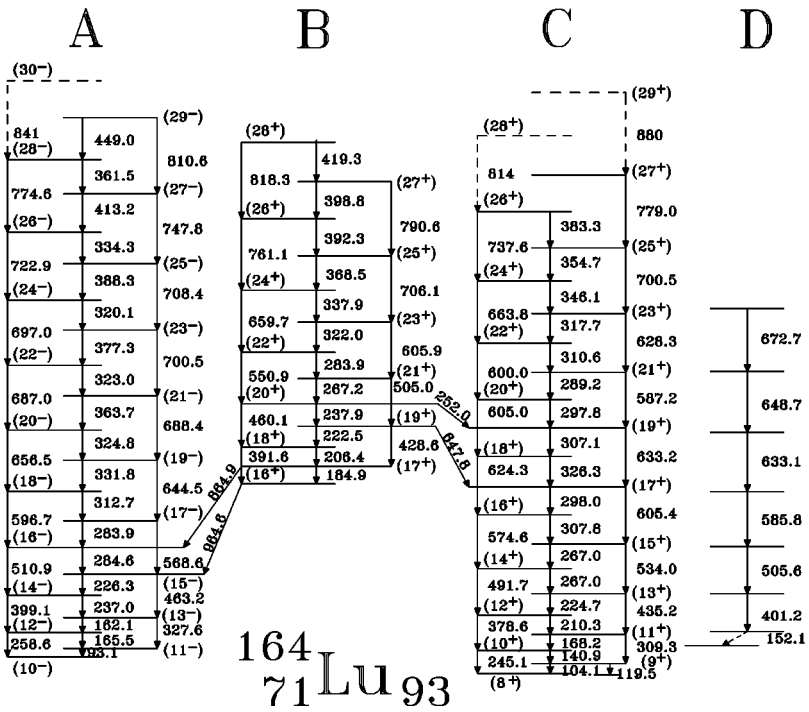

FIG. 7. Level scheme of ^{164}Lu proposed in the present work.

Tables I and II was evaluated. For low lying $\Delta I=1$ transitions in the yrast band of ^{162}Lu, mixing ratios δ were estimated from angular correlation measurements to be less than 0.27, so it produces a small influence in the $B(M1)/B(E2)$ ratios. The experimental $B(M1)/B(E2)$ ratios, determined assuming $\delta^2=0$, and the branching ratios are included in Tables I and II for ^{162}Lu and ^{164}Lu, respectively.

III. DISCUSSION

Proton and neutron orbitals involved in rotational bands found in ^{162}Lu and ^{164}Lu can be identified on the basis of the coupling schemes proposed by Kreiner and co-workers [26–28]. For each odd-odd nucleus, the first step is the construction of a zero-order level scheme from experimental bandhead energies in neighboring odd-A nuclei. Figure 9 shows the evolution of these energies as a function of the neutron number in odd Lu [22–24,29–32] and Yb [33–36] isotopes. No experimental data concerning bandhead energies exist for ^{161}Lu ($N=90$) [21], but the tendency is quite clear. In the $h_{11/2}$ proton bands the Fermi level is located near $\Omega=9/2$ ($9/2^-[514]$) in ^{165}Lu [23] and seems to be located between the $\Omega=7/2$ ($7/2^-[523]$) and $\Omega=9/2$ ($9/2^-[514]$) in ^{163}Lu [22,29]. On the other hand, Rosenthal [37] and Waddington *et al.* [38] proposed $I^\pi=1/2^-$ for the ground state of ^{163}Lu. The only negative-parity proton orbital with $\Omega=1/2$

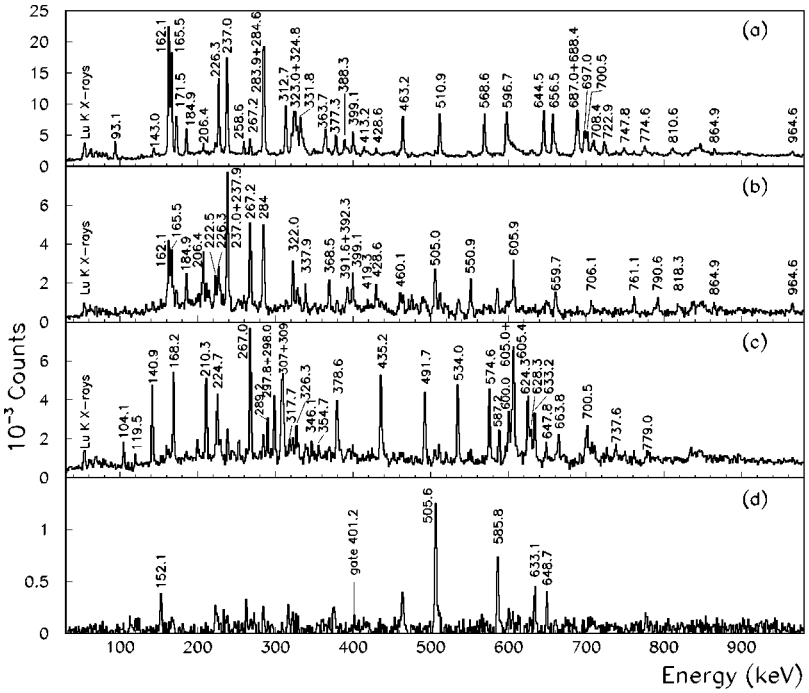

FIG. 8. γ-ray coincidence spectra corresponding to the sum of several gates on transitions belonging to band A (a), band B (b), and band C (c) of ^{164}Lu. (d) γ-ray coincidence spectrum obtained with gate on the 401.2 keV transition belonging to band D.

TABLE II. γ-ray transition energies, spin assignments, γ intensities, branching ratios, DCO ratios, and $B(M1)/B(E2)$ ratios in ^{164}Lu.

E_γ (keV) [a]	$I_i^\pi \rightarrow I_f^\pi$ [b]	I_γ [c]	Branching ratio [d]	DCO ratio [e]	$B(M1)/B(E2)$ [f] (μ_N^2/e^2b^2)
Band A					
93.1	$(11^-)\rightarrow(10^-)$	219		0.74±0.12	
165.5	$(12^-)\rightarrow(11^-)$	1000	0.16±0.02	0.71±0.06	1.10±0.14
258.6	$(12^-)\rightarrow(10^-)$	144			
162.1	$(13^-)\rightarrow(12^-)$	1100	0.33±0.07	0.74±0.06	1.9±0.4
327.6	$(13^-)\rightarrow(11^-)$	330		1.2±0.2	
237.0	$(14^-)\rightarrow(13^-)$	1043	0.50±0.08		1.05±0.17
399.1	$(14^-)\rightarrow(12^-)$	500		1.10±0.20	
226.3	$(15^-)\rightarrow(14^-)$	821	1.0±0.1	0.65±0.05	1.28±0.13
463.2	$(15^-)\rightarrow(13^-)$	894		1.19±0.13	
284.6	$(16^-)\rightarrow(15^-)$	744	0.91±0.11	0.78±0.15	1.15±0.14
510.9	$(16^-)\rightarrow(14^-)$	790		0.93±0.12	
283.9	$(17^-)\rightarrow(16^-)$	528	1.6±0.3	0.74±0.10	1.12±0.21
568.6	$(17^-)\rightarrow(15^-)$-	785		0.97±0.15	
312.7	$(18^-)\rightarrow(17^-)$	492	1.5±0.2	0.68±0.10	1.14±0.15
596.7	$(18^-)\rightarrow(16^-)$	770		1.0±0.2	
331.8	$(19^-)\rightarrow(18^-)$	364	2.5±0.4		0.84±0.14
644.5	$(19^-)\rightarrow(17^-)$	727		1.08±0.15	
324.8	$(20^-)\rightarrow(18^-)$	326	1.7±0.3		1.5±0.3
656.5	$(20^-)\rightarrow(19^-)$	566		1.2±0.2	
363.7	$(21^-)\rightarrow(20^-)$	288	2.0±0.4	0.69±0.17	1.11±0.22
688.4	$(21^-)\rightarrow(19^-)$	568		1.10±0.18	
323.0	$(22^-)\rightarrow(21^-)$	306	2.4±0.6		1.3±0.3
687.0	$(22^-)\rightarrow(20^-)$	597		1.3±0.2	
377.3	$(23^-)\rightarrow(22^-)$	159	2.2±0.4	0.67±0.20	1.0±0.2
700.5	$(23^-)\rightarrow(21^-)$	361			
320.1	$(24^-)\rightarrow(23^-)$	212	1.9±0.3	0.60±0.12	1.8±0.3
697.0	$(24^-)\rightarrow(22^-)$	394			
388.3	$(25^-)\rightarrow(24^-)$	154	1.5±0.3	0.75±0.21	1.4±0.3
708.4	$(25^-)\rightarrow(23^-)$	222			
334.3	$(26^-)\rightarrow(25^-)$	110	1.6±0.4	0.79±0.25	2.3±0.6
722.9	$(26^-)\rightarrow(24^-)$	199		1.2±0.2	
413.2	$(27^-)\rightarrow(26^-)$	94	1.1±0.3		2.1±0.6
747.8	$(27^-)\rightarrow(25^-)$	107			
361.5	$(28^-)\rightarrow(27^-)$	70	1.7±0.6		2.4±0.8
774.6	$(28^-)\rightarrow(26^-)$	144			
449.0	$(29^-)\rightarrow(28^-)$	40	1.4±0.5		1.9±0.7
810.6	$(29^-)\rightarrow(27^-)$	54			
841	$(30^-)\rightarrow(28^-)$				
Band B					
184.9	$(17^+)\rightarrow(16^+)$	33			
206.4	$(18^+)\rightarrow(17^+)$	98	0.45±0.08		1.6±0.3
391.6	$(18^+)\rightarrow(16^+)$	83			
222.5	$(19^+)\rightarrow(18^+)$	78	0.59±0.09	0.81±0.21	1.5±0.2
428.6	$(19^+)\rightarrow(17^+)$	45			
237.9	$(20^+)\rightarrow(19^+)$	80	0.77±0.15		1.4±0.3
460.1	$(20^+)\rightarrow(18^+)$	64		0.94±0.26	
267.2	$(21^+)\rightarrow(20^+)$	66	0.94±0.15		1.3±0.2
505.0	$(21^+)\rightarrow(19^+)$	64			
283.9	$(22^+)\rightarrow(21^+)$	90	0.67±0.10		2.3±0.3
550.9	$(22^+)\rightarrow(20^+)$	67			
322.0	$(23^+)\rightarrow(22^+)$	55	1.4±0.3	0.84±0.25	1.2±0.3
605.9	$(23^+)\rightarrow(21^+)$	82			
337.9	$(24^+)\rightarrow(23^+)$	44	1.7±0.3		1.3±0.2
659.7	$(24^+)\rightarrow(22^+)$	52			
368.5	$(25^+)\rightarrow(24^+)$	27	2.5±0.6		0.97±0.23
706.1	$(25^+)\rightarrow(23^+)$	63			
392.3	$(26^+)\rightarrow(25^+)$	22	2.0±0.4		1.5±0.3
761.1	$(26^+)\rightarrow(24^+)$	40			
398.8	$(27^+)\rightarrow(26^+)$	14	3.2±0.8		1.1±0.3
790.6	$(27^+)\rightarrow(25^+)$	40			
419.3	$(28^+)\rightarrow(27^+)$	5	2.8±0.6		1.2±0.3
818.3	$(28^+)\rightarrow(26^+)$	17			

TABLE II. (*Continued*).

E_γ (keV) [a]	$I_i^\pi \rightarrow I_f^\pi$ [b]	I_γ [c]	Branching ratio [d]	DCO ratio [e]	$B(M1)/B(E2)$ [f] (μ_N^2/e^2b^2)
Transitions between A and B					
864.9	$(17^+)\rightarrow(16^-)$	61		$\leqslant 0.6$	
964.6	$(16^+)\rightarrow(15^-)$	101		$\leqslant 0.7$	
Band C					
104.1	$(9^+)\rightarrow(8^+)$	87		0.62 ± 0.15	
140.9	$(10^+)\rightarrow(9^+)$	229	0.21 ± 0.05	0.60 ± 0.12	1.0 ± 0.2
245.1	$(10^+)\rightarrow(8^+)$	43			
168.2	$(11^+)\rightarrow(10^+)$	295	0.56 ± 0.07	0.62 ± 0.12	0.74 ± 0.09
309.3	$(11^+)\rightarrow(9^+)$	160			
210.3	$(12^+)\rightarrow(11^+)$	338	0.83 ± 0.13	0.72 ± 0.14	0.70 ± 0.11
378.6	$(12^+)\rightarrow(10^+)$	268		1.1 ± 0.2	
224.7	$(13^+)\rightarrow(12^+)$	219	1.6 ± 0.2		0.60 ± 0.07
435.2	$(13^+)\rightarrow(11^+)$	298		1.19 ± 0.15	
267.0	$(14^+)\rightarrow(13^+)$	135	1.9 ± 0.3	0.56 ± 0.20	0.55 ± 0.09
491.7	$(14^+)\rightarrow(12^+)$	292		0.96 ± 0.19	
267.0	$(15^+)\rightarrow(14^+)$	140	2.4 ± 0.7	0.76 ± 0.23	0.66 ± 0.19
534.0	$(15^+)\rightarrow(13^+)$	371		0.97 ± 0.16	
307.8	$(16^+)\rightarrow(15^+)$	103	2.9 ± 0.8		0.51 ± 0.14
574.6	$(16^+)\rightarrow(14^+)$	325		0.8 ± 0.3	
298.0	$(17^+)\rightarrow(16^+)$	80	6.3 ± 1.8		0.34 ± 0.10
605.4	$(17^+)\rightarrow(15^+)$	530			
326.3	$(18^+)\rightarrow(17^+)$	76	7.1 ± 1.7		0.27 ± 0.06
624.3	$(18^+)\rightarrow(16^+)$	285		1.3 ± 0.3	
307.1	$(19^+)\rightarrow(18^+)$	72	3.1 ± 0.7		0.79 ± 0.18
633.2	$(19^+)\rightarrow(17^+)$	242		1.2 ± 0.3	
297.8	$(20^+)\rightarrow(19^+)$	91	0.9 ± 0.3		2.4 ± 0.8
605.0	$(20^+)\rightarrow(18^+)$	80			
289.2	$(21^+)\rightarrow(20^+)$	56	1.1 ± 0.3		1.8 ± 0.5
587.2	$(21^+)\rightarrow(19^+)$	76			
310.6	$(22^+)\rightarrow(21^+)$	60	1.5 ± 0.3		1.2 ± 0.2
600.0	$(22^+)\rightarrow(20^+)$	78			
317.7	$(23^+)\rightarrow(22^+)$	33	2.9 ± 0.7		0.73 ± 0.18
628.3	$(23^+)\rightarrow(21^+)$	99			
346.1	$(24^+)\rightarrow(23^+)$	33	5.0 ± 1.2		0.43 ± 0.11
663.8	$(24^+)\rightarrow(22^+)$	163			
354.7	$(25^+)\rightarrow(24^+)$	23	4.4 ± 0.8		0.60 ± 0.12
700.5	$(25^+)\rightarrow(23^+)$	119			
383.3	$(26^+)\rightarrow(25^+)$	21	3.5 ± 0.6		0.78 ± 0.16
737.6	$(26^+)\rightarrow(24^+)$	102			
779.0	$(27^+)\rightarrow(25^+)$	107			
814	$(28^+)\rightarrow(26^+)$	14			
880	$(29^+)\rightarrow(27^+)$	23			
Transitions between B and C					
647.8	$(19^+)\rightarrow(17^+)$	118		1.1 ± 0.2	
252.0	$(20^+)\rightarrow(19^+)$	30			
Band D					
401.2		160		1.2 ± 0.2	
505.6		145			
585.8		116			
633.1		76			
648.7		54			
672.7		15			

[a]Uncertainties between 0.1 and 0.3 keV.

[b]Spin assignment based on systematics.

[c]Intensities extracted from the ^{139}La(^{29}Si,4n) reaction at 145 MeV. Uncertainties between 5 and 30 %.

[d]Branching ratio: $I\gamma(I\rightarrow I-2)/I\gamma(I\rightarrow I-1)$, $I\gamma(I\rightarrow I-2)$, and $I\gamma(I\rightarrow I-1)$ are the relative γ intensities of the quadrupole and dipole transition depopulating the spin I level, respectively.

[e]Directional correlation ratio: $I\gamma_{\text{gate}=\theta_2}(\theta_1)/I\gamma_{\text{gate}=\theta_1}(\theta_2)$, ($\theta_1\approx 32°$, 36°, 144°, and 148°, and $\theta_2=90°$) determined from coincidence spectra, setting gates on stretched $E2$ transitions on both axes of the DCO matrix.

[f]Determined assuming $\delta^2=0$.

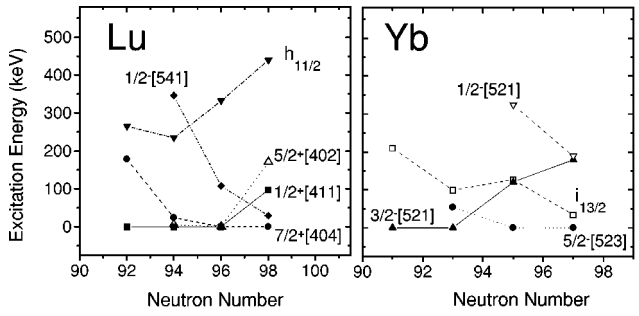

FIG. 9. Bandhead excitation energies for odd Lu and Yb isotopes.

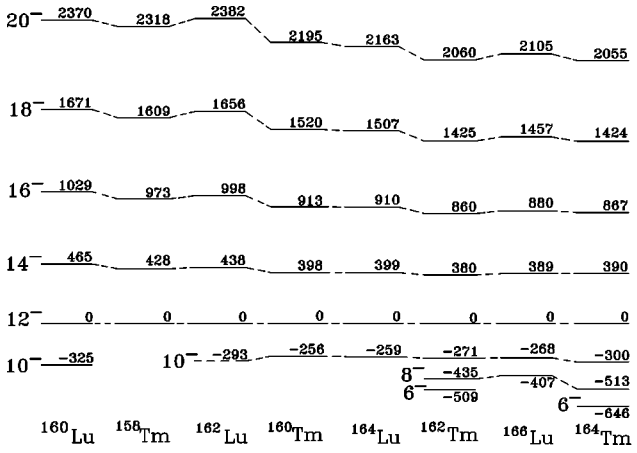

FIG. 10. Systematics of the $\alpha=0$ sequences for the $\pi h_{11/2}\otimes \nu i_{13/2}$ structure in $^{160-166}$Lu and $^{158-164}$Tm.

in this region is $1/2^-[541]$ but its energy increases as the neutron number decreases, lying at about 350 keV in ^{165}Lu. In this context we agree with Rastikerdar *et al.* [39] in assigning the $1/2^+[411]$ orbital to the ground state of ^{163}Lu (see Ref. [30]). In addition, in neutron $i_{13/2}$ bands, the Fermi level lies close to $\Omega=5/2$ ($5/2^+[642]$) in ^{163}Yb and to $\Omega=3/2$ ($3/2^+[651]$) in ^{161}Yb. To a zero-order approximation proton and neutron single-quasiparticle energies are added, neglecting the residual interaction which can split the $K_\pm=|\Omega_p\pm\Omega_n|$ states according to the Gallagher-Moszkowski coupling rules [40]. Table III shows the results obtained for ^{164}Lu, which must be approximately valid for ^{162}Lu given the relatively smooth variation of quasiparticle energies with neutron number.

A. Bands A, yrast bands

The most strongly populated bands in ^{162}Lu and ^{164}Lu are those labeled A in Figs. 5 and 7. These bands, already reported in Ref. [14], exhibit a pronounced level staggering and a signature inversion, characteristic of the $\pi h_{11/2}\otimes \nu i_{13/2}$ bands in this mass region. These bands can be described as semidecoupled, because the neutron is quite decoupled (relatively large $\Omega_n=1/2$ component) giving rise to decoupled bands in odd neutron nuclei, while the proton is more strongly coupled ($\Omega_p=9/2,7/2$) but Coriolis perturbed. A characteristic feature of these structures (extensively studied in $\pi h_{9/2}\otimes \nu i_{13/2}$ systems [41]) is that they start with multiplets formed by low-energy highly converted $M1$ transitions. The lower transitions of this kind of band are often unobserved, possibly due to the compression caused by the neutron $i_{13/2}$ and the irregularity of the states with $I<j$ in $h_{11/2}$ bands, leading generally to low-energy highly converted transitions. The band head spins are expected to be 6 or 5 for ^{162}Lu and 7 or 6 for ^{164}Lu (see Table III), but in order to assign spins to the lower observed states, we must base these assignments on systematics. Figure 10 displays the $\alpha=0$ sequence of $\pi h_{11/2}\otimes \nu i_{13/2}$ bands belonging to $^{158-164}$Tm [11] and $^{160-166}$Lu [1,42] isotopes. We use the 12^- state ($12=J_{\max}=j_p+j_n$) as reference. On this basis, the most probable spin for the lower observed state of bands A is 10 in both cases. Only a change of two units of spin is possible, due to the fact that the even-spin sequences correspond to the favored signature ($\alpha=0$) for high spin states.

In the upper part of Figs. 11(a) and 11(b) we plot the normalized $\Delta I=1$ transition energies as a function of spin

TABLE III. Zero-order level scheme of ^{164}Lu. Entries are $K_\pm=|\Omega_p\pm\Omega_n|$ values and zero-order energies in keV. Proton excitation energies correspond to the average between ^{163}Lu and ^{165}Lu (except for the $\pi 1/2[541]$ orbital; the 345.3 keV value belongs to ^{165}Lu and for ^{163}Lu is expected to be higher). Neutron excitation energies are from ^{163}Yb.

$\pi\Omega_p^\pi[Nn_3\Lambda]$ E_π (keV)	$\nu\Omega_n^\pi[Nn_3\Lambda]$ E_ν (keV)	$\nu 3/2^-[521]$ 0.0	$\nu 5/2^-[523]$ 53.9	$\nu i_{13/2}$ $\nu 5/2^+[642]$ 99.2
$\pi 7/2^+[404]$		$5^-, 2^-$	$6^-, 1^-$	$6^+, 1^+$
100.7		100.7	154.6	199.9
$\pi h_{11/2}$				
$\pi 9/2^-[514](\pi 7/2^-[523])$		$6(5)^+, 3(2)^+$	$7(6)^+, 2(1)^+$	$7(6)^-, 2(1)^-$
249.0		249.0	302.9	348.2
$\pi 1/2^+[411]$		$2^-, 1^-$	$3^-, 2^-$	$3^+, 2^+$
0.0		0.0	53.9	99.2
$\pi 1/2^-[541]$		$2^+, 1^+$	$3^+, 2^+$	$3^-, 2^-$
$\geqslant$345.3		$\geqslant$345.3	$\geqslant$399.2	$\geqslant$444.5

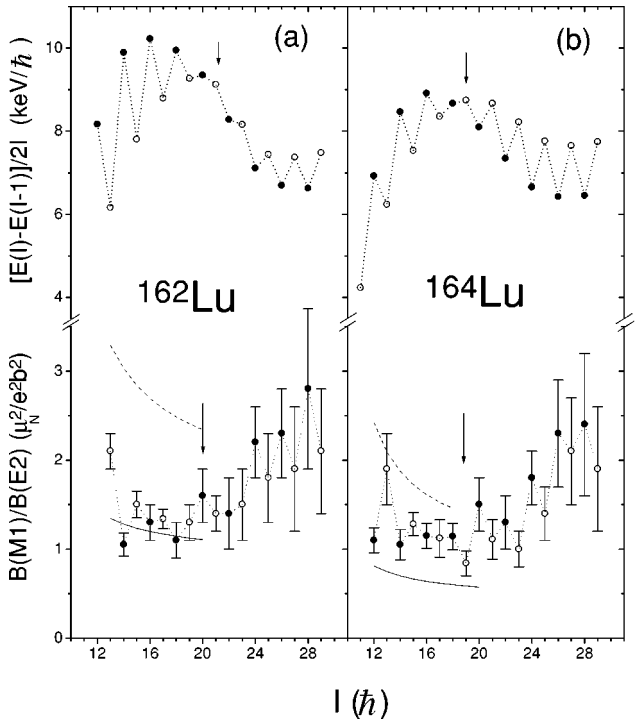

FIG. 11. Level staggering and $B(M1)/B(E2)$ values as a function of the angular momentum for the yrast band of ^{162}Lu (a) and ^{164}Lu (b). Solid (open) circles correspond to $\alpha=0(1)$ states. The arrows point at the position of the signature inversion. In the lower part the calculated $B(M1)/B(E2)$ values have been plotted with a solid line for the $\pi h_{11/2}(7/2^-[523])\otimes\nu i_{13/2}(3/2^+[651])$ configuration in ^{162}Lu (a) and $\pi h_{11/2}(7/2^-[523])\otimes\nu i_{13/2}(5/2^+[642])$ configuration in ^{164}Lu (b), and a dashed line for the $\pi h_{11/2}(9/2^-[514])\otimes\nu i_{13/2}(3/2^+[651])$ configuration in ^{162}Lu (a) and $\pi h_{11/2}(9/2^-[514])\otimes\nu i_{13/2}(5/2^+[642])$ configuration in ^{164}Lu (b).

for bands A of ^{162}Lu and ^{164}Lu, respectively. At high spins, namely, above the signature inversion point, states with even spin are favored, corresponding to the coupling between the favored signatures in both proton ($\alpha^f=-1/2$) and neutron ($\alpha^f=+1/2$) orbitals. This assumption is consistent with the dominance of the Coriolis force over other possible ingredients [41], such as the *p-n* residual force, for sufficiently high spins. A similar behavior (staggering and signature inversion) can be observed for the experimental $B(M1)/B(E2)$ ratios [lower part of Figs. 11(a) and 11(b)]. The uncertainty in these values is important, but the effect seems to be quite clear. This behavior is mainly due to the level staggering. In Fig. 11 the arrows indicate the point of the staggering phase change. In Ref. [14] we have shown the systematic variation of the level staggering and signature inversion features for all $\pi h_{11/2}\otimes\nu i_{13/2}$ known bands in the light rare-earth region. The evolution of the phase change in the level staggering is plotted in Fig. 12. To avoid possible errors in the spin assignments often based on systematics, the frequency value at the signature inversion point was considered. Figure 12(a) shows that for each isotopic chain the inversion frequency decreases with the neutron number. In Fig. 12(b) the behavior of the isotones is presented, in this case for a fixed neutron number the inversion frequency increases with Z. A similar study has been undertaken in Ref. [43]. We have not

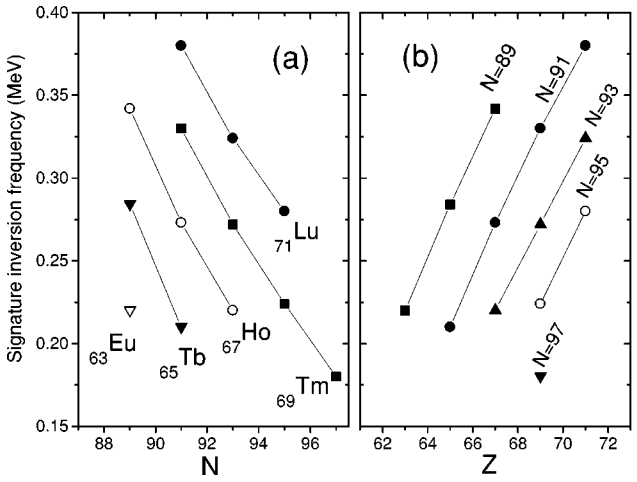

FIG. 12. Evolution of the signature inversion frequency observed in the level staggering of the $\pi h_{11/2}\otimes\nu i_{13/2}$ structure for the isotopes (a) and isotones (b) belonging to the light rare-earth region.

been able to come up with a plausible explanation of the trend observed for the signature inversion frequency. If we assume that the phase of the staggering beyond the inversion point corrresponds to a dominance of the signature-dependent Coriolis interaction [44], we would expect a decrease in the amplitude of the level staggering (beyond the inversion point) as the deformation increases. However, just the opposite seems to be occurring (see Fig. 2 of Ref. [14]). For instance for $N=91$, i.e., the series of nuclei ^{162}Lu, ^{160}Tm, ^{158}Ho, and ^{156}Tb (Fig. 13), as Z decreases (and the deformation β increases as can be seen from Fig. 14) the amplitude of the signature oscillation (above the inversion point) increases. On the other hand, the behavior of the amplitude of the oscillation before the inversion point is opposite to the one beyond, suggesting perhaps a different origin for both phenomena. In Fig. 14 the β values were obtained from experimental lifetimes of the 2^+ state in even-even nuclei (Refs. [25,45–53]).

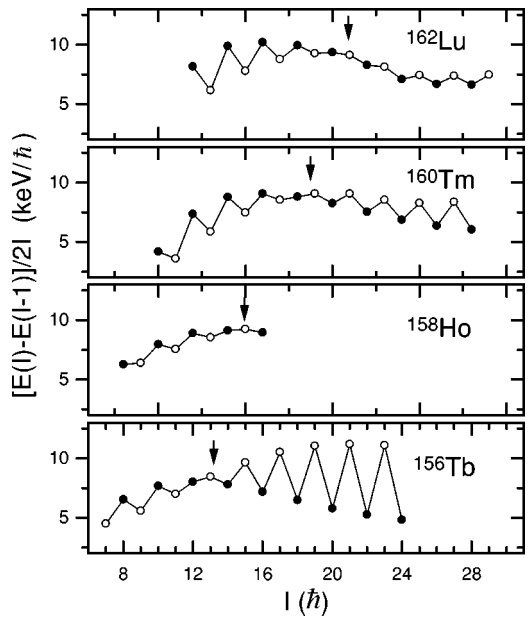

FIG. 13. Level staggering of the $\pi h_{11/2}\otimes\nu i_{13/2}$ structure in the $N=91$ isotone chain, the arrows point at the phase change.

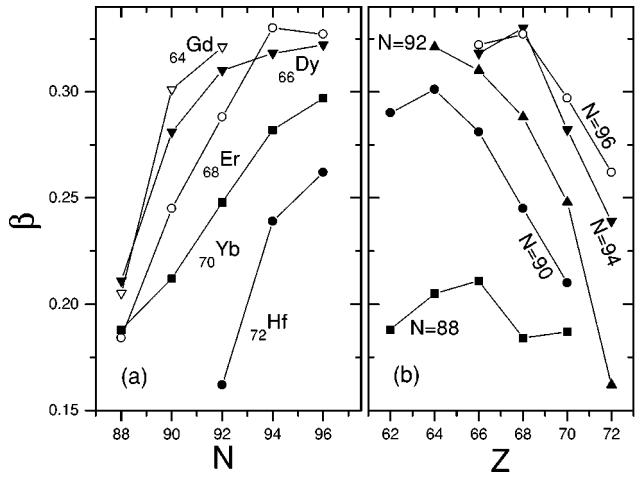

FIG. 14. Evolution of quadrupole deformation β in the mass region of interest. The β values were obtained from experimental lifetimes of the 2^+ state in the even-even nuclei.

In the lower part of Fig. 11 the experimental $B(M1)/B(E2)$ ratios are compared with the values calculated in the framework of the cranking model, as discussed in Sec. IV. Calculations have been performed using two different values of Ω_p (7/2 and 9/2) and the corresponding alignments and g factors (see Table IV). Due to the degree of precision of the method, no firm conclusion can be extracted as to which Ω_p is predominantly involved in the structures of bands A. For the yrast band of ^{162}Lu the theoretical ratios for the $\pi h_{11/2}(7/2^-[523])\otimes\nu i_{13/2}(3/2^+[651])$ configuration are in very good agreement with the experimental values. It should be remarked, however, that the calculational approach is semiclassical. For both nuclei the general trend of the variation of $B(M1)/B(E2)$ values as a function of the angular momentum is very similar. These values are almost constant around $\approx 1.2\mu_N^2/e^2\mathrm{b}^2$ up to $I\approx 20\hbar$ ($\hbar\omega\approx 0.340$ -0.380 MeV) above this point a smooth increase is observed. The behavior of the $B(M1)/B(E2)$ values has been discussed recently for the $\pi h_{11/2}\otimes\nu i_{13/2}$ structures in ^{160}Ho [43,54] and ^{166}Tm [55] as a function of frequency showing a characteristic parabolalike trend with the increase of the ratios above 0.25 and 0.20 MeV for ^{160}Ho and ^{166}Tm, respectively. These frequencies are quite smaller than the ones mentioned above for ^{162}Lu and ^{164}Lu. In the odd-Z nuclei

TABLE IV. Parameters used in the calculations of $B(M1)$ values. The alignments are extracted from $^{161(163)}$Lu and $^{161(163)}$Yb for the proton and neutron orbital in $^{162(164)}$Lu, respectively, and correspond to the favored signature.

Orbital	^{162}Lu $i(\hbar)$	^{162}Lu g_Ω	^{164}Lu $i(\hbar)$	^{164}Lu g_Ω
$\pi 7/2^-[523]$	3.0	1.31	2.7	1.32
$\pi 9/2^-[514]$	2.2	1.29	2.2	1.29
$\pi 7/2^+[704]$			0.52	0.634
$\nu 3/2^+[651]$	5.8	-0.295		
$\nu 5/2^+[642]$			5.2	-0.279
$\nu 3/2^-[521]$			1.5	-0.208
$\nu 5/2^-[523]$			0.93	0.167

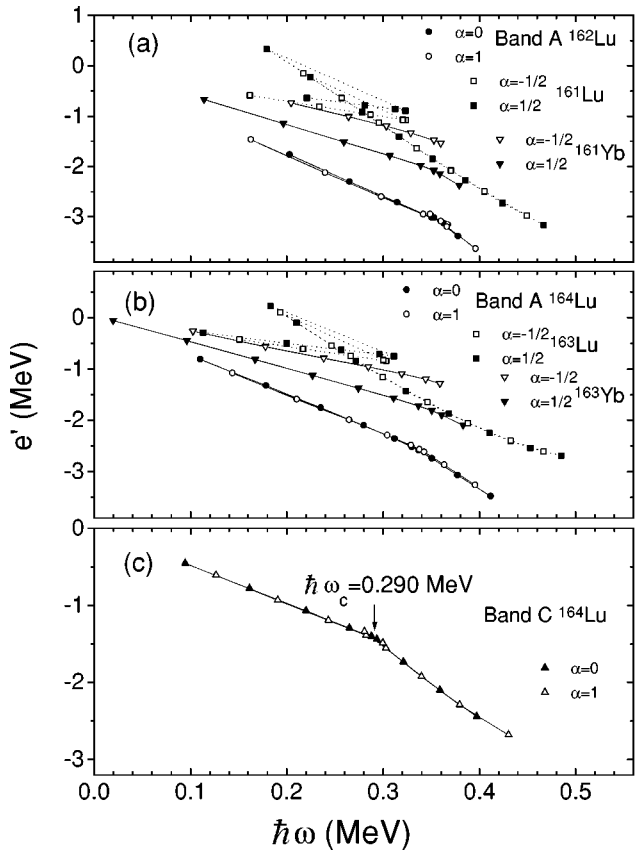

FIG. 15. Experimental Routhians of the $\pi h_{11/2}$, $\nu i_{13/2}$, and $\pi h_{11/2}\otimes\nu i_{13/2}$ (band A) structures in ^{161,163}Lu, ^{161,163}Yb, and ^{162,164}Lu, respectively and of band C of ^{164}Lu as a function of the rotational frequency. For these bands the moments of inertia used for the reference configuration are reported in Table V, except for band C of ^{164}Lu, for which the inertia parameters are $J_0/\hbar^2=26.7$ MeV^{-1} and $J_1/\hbar^4=126.2$ MeV^{-3}.

^{161}Lu and ^{163}Lu more dramatic changes occur at the frequency of the $i_{13/2}$ neutron band crossing. In ^{161}Lu [21] an increase from a $B(M1)/B(E2)$ value around 0.5 $\mu_N^2/e^2\mathrm{b}^2$ at low spin to 2.5 $\mu_N^2/e^2\mathrm{b}^2$ after the band crossing was observed, which has been associated with the alignment of a pair of $i_{13/2}$ neutrons.

Two additivity effects have been analyzed in these bands. The first one corrresponds to the crossing frequency shifts ($\delta\hbar\omega_c$) [6]. Figures 15(a) and 15(b) shows the experimental Routhians as a function of the rotational frequency for bands A of ^{162,164}Lu, the $\pi h_{11/2}$ bands in ^{161,163}Lu, and the $\nu i_{13/2}$ bands in ^{161,163}Yb [30,56]. The crossing frequencies associated with the alignment of a pair of $i_{13/2}$ neutrons extracted from the Routhians are reported in Table V along with the moments of inertia used for the reference configuration and alignments. In order to extract appropriate single quasiparticle parameters from a given band (such as alignment), the associated core (or the so-called reference) parameters have to be determined in each band separately, since every configuration can affect the core through blocking, polarization, etc., differently. The analysis has been performed using both $\Omega_p=7/2$ and $\Omega_p=9/2$ for the orbital of the odd proton. While the occupation of the $i_{13/2}$ neutron orbital in ^{161,163}Yb produces an important delay in the crossing frequency with respect to the corresponding even-even core

TABLE V. Moments of inertia, alignments (for odd nuclei the reported values correspond to the favored signature), calculated alignment ($i^{\rm calc}=i_n+i_p$), band-crossing frequencies, experimental and calculated deviations of the crossing frequencies with respect to the even-even core [ground state (g.s.) band]. The calculated deviations $\delta\hbar\omega_c^{\rm calc}$ are obtained summing the deviations of the odd-N and odd-Z neighboring nuclei.

Nucleus	Band	$J_0/\hbar^2$ (MeV^{-1})	$J_1/\hbar^4$ (MeV^{-3})	i ($\hbar$)	$i^{\rm calc}$ ($\hbar$)	$\hbar\omega_c$ (MeV)	$\delta\hbar\omega_c$ (MeV)	$\delta\hbar\omega_c^{\rm calc}$ (MeV)
^{160}Yb	g.s. band	9.7	186.2			0.270(5)		
^{161}Yb	$i_{13/2}(3/2^+[651])$	17.1	100.9	5.8		0.355(15)	+0.085	
^{161}Lu	$h_{11/2}(7/2^-[523])$	15.0	135.3	3.0		0.270(5)	0.0	
	$h_{11/2}(9/2^-[514])$	19.5	123.0	2.2		0.265(5)	-0.005	
^{162}Lu	$A\Omega_p=7/2$	15.2	118.8	8.4	8.8	0.355(5)	+0.085	+0.085
	$A\Omega_p=9/2$	19.0	96.5	7.5	8.0	0.350(5)	+0.080	+0.080
^{162}Yb	g.s. band	16.8	177.2			0.270(5)		
^{163}Yb	$i_{13/2}(5/2^+[642])$	24.3	93.6	5.2		0.355(10)	+0.085	
^{163}Lu	$h_{11/2}(7/2^-[523])$	18.9	145.8	2.7		0.260(10)	-0.010	
	$h_{11/2}(9/2^-[514])$	22.2	127.7	2.2		0.250(10)	-0.020	
^{164}Lu	$A\Omega_p=7/2$	21.8	117.8	7.4	7.9	0.335(5)	+0.065	+0.075
	$A\Omega_p=9/2$	25.0	111.3	6.7	7.4	0.330(5)	+0.060	+0.065

^{160,162}Yb [50,51,57] (0.085 MeV) most likely due to blocking, the presence of the odd proton has a negligible effect in ^{161}Lu and in ^{163}Lu produces a reduction in the crossing frequency. In band A of $^{162(164)}$Lu the crossing occurs at a frequency of $\hbar\omega_c\approx 0.35(0.33)$ MeV, and the shift in the crossing frequency is in very good agreement with the sum of the shifts in the crossing frequencies for the odd N and odd Z neighboring nuclei (Table V).

The second additivity effect corresponds to alignments. Figures 16(a) and 16(b) show the alignments of the bands mentioned before (the values of bands B are also plotted but discussed below). For ^{161,163}Yb and band A of ^{162,164}Lu the data are referred to a reference configuration having the moments of inertia listed in Table V. For ^{161,163}Lu two sets of inertia parameters were used, the one listed in Table V for the region below the backbending and above the backbending we used: $J_0/\hbar^2=33.8(27.0)$ MeV^{-1} and $J_1/\hbar^4=31.4(45.2)$ MeV^{-3} for $^{161(163)}$Lu. For the odd nuclei ^{161,163}Lu and ^{161,163}Yb the alignment values of the favored signature sequence are reported in Table V. A very small signature splitting effect is observed in the alignment of bands A for both nuclei ^{162,164}Lu, and this value below the backbending is very close to the sum of the values corresponding to the neighboring odd nuclei ($i^{\rm calc}$) (see Table V). Above the backbending the alignment gains are $6.3\hbar$ and $4.8\hbar$ for ^{162}Lu and ^{164}Lu, respectively: these values are close to the corresponding ones found in the $i_{13/2}$ bands of ^{161}Yb and ^{163}Yb ($6.2\hbar$ and $4.2\hbar$, respectively).

B. Bands B

Proton $7/2^+[404]$ bands have been reported in ^{161,163}Lu [21,22]. While in ^{163}Lu the band has been identified from the bandhead, in ^{161}Lu only states above the $i_{13/2}$ quasineutron band crossing have been established.

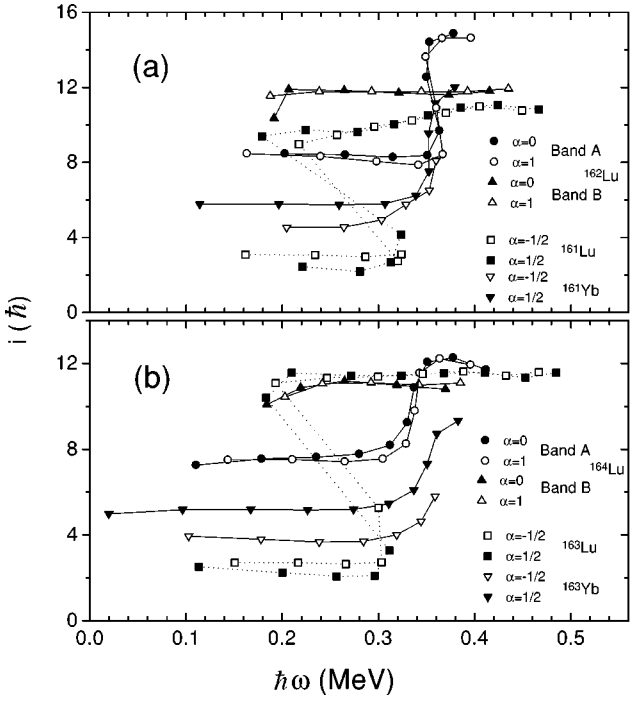

FIG. 16. Experimental alignments of the $\pi h_{11/2}$, $\nu i_{13/2}$, and $\pi h_{11/2}\otimes\nu i_{13/2}$ (band A) structures in ^{161,163}Lu, ^{161,163}Yb, and ^{162,164}Lu, respectively as a function of the rotational frequency. The moments of inertia used for the $\nu i_{13/2}$ band of ^{161,163}Yb, the $\pi h_{11/2}$ band of ^{161,163}Lu (below the backbending), and band A of ^{162,164}Lu are reported in Table V. For $^{161(163)}$Lu the parameters used above the backbending are $J_0/\hbar^2=33.8(27.0)$ MeV^{-1} and $J_1/\hbar^4=31.4(45.2)$ MeV^{-3}. The alignment values corresponding to band B of $^{162(164)}$Lu determined using $J_0/\hbar^2=32.7(33.6)$ MeV^{-1} and $J_1/\hbar^4=23.1(31.0)$ MeV^{-3} as reference core parameters are also shown.

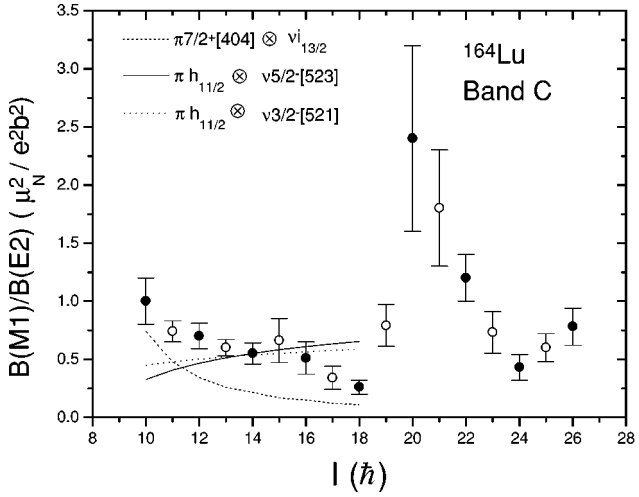

FIG. 17. Experimental $B(M1)/B(E2)$ values corresponding to band C of ^{164}Lu and the results of the calculations obtained in the framework of the cranking model for the possible positive configurations. For the $\pi_{11/2}$ the orbital $7/2^-[523]$ was considered.

In addition, in both nuclei the first states above the backbending are linked to the $h_{11/2}$ band through $E1$ transitions. The analogy with bands B of ^{162,164}Lu seems clear. The lower observed states of bands B decay to bands A through $E1$ transitions of very similar energies. In doubly odd ^{166}Lu the intrinsic state of $\pi 7/2^+[404]$ coupled to $\nu i_{13/2}$ was identified at an excitation energy of 190 keV [1]. This configuration is also expected in ^{162,164}Lu (see Table III). The experimental alignments of bands B in $^{162(164)}$Lu were determined using $J_0/\hbar^2=32.7(33.6)$ MeV^{-1} and $J_1/\hbar^4=23.1(31.0)$ MeV^{-3} as reference core parameters. If we compare the alignments obtained for bands B (i_B) (see Fig. 16) with the addition of those corresponding to $\pi 7/2^+[404]$ (i_p), estimated from ^{165,167}Lu and the $\nu i_{13/2}$ bands (i_n), and the alignment gain in bands A above the backbending (i_{nn}), we obtain a very good agreement, i.e., for ^{162}Lu,

$$i_p+i_n+i_{nn}=0.5\hbar+5.8\hbar+6.3\hbar=12.6\hbar \quad \text{vs} \quad i_B=11.9\hbar,$$

and

$$i_p+i_n+i_{nn}=0.5\hbar+5.2\hbar+4.8\hbar$$
$$=10.5\hbar \quad \text{vs} \quad i_B=10.9\hbar \quad \text{for } ^{164}\text{Lu}.$$

On this basis we identified the band B in ^{162,164}Lu as a four-quasiparticle band probably involving the configuration $\pi 7/2^+[404]\otimes\nu i_{13/2}\otimes(\nu i_{13/2})^2$.

C. Band C of ^{164}Lu

As has been already pointed out in this work the stretched $E2$ character of the 647.8 keV linking transition fixes the spin and parity of band C relative to band B. In this way positive parity and a spin sequence as shown in the level scheme (Fig. 7) has been assigned to band C, which differs by one unit from that reported by Juneja *et al.* [18]. Because of the positive parity of band C only three configurations can be associated to this band: (a) $\pi h_{11/2}\otimes\nu 3/2^-[521]$, (b) $\pi h_{11/2}\otimes\nu 5/2^-[523]$, and (c) $\pi 7/2^+[404]\otimes\nu i_{13/2}$. Figure 17 shows the experimental $B(M1)/B(E2)$ values corresponding to band C compared with the calculated ones (see Sec. IV and Table IV) for the possible positive parity configurations. Good agreement is obtained for the configurations (a) and (b) mentioned above. The configuration $\pi 7/2^+[404]\otimes\nu i_{13/2}$, which, on the other hand, has been already assigned to bands B, must involve an important delay in the crossing frequency. However, if we compare the crossing frequencies extracted from Routhians for band C of ^{164}Lu, $\hbar\omega_c=0.290$ MeV [Fig. 15(c)] and for the ground-state band of the even-even core (^{162}Yb), $\hbar\omega_c=0.270$ MeV (Table V), the observed delay is inconsistent with this configuration. From this analysis no conclusion can be made about which neutron orbital, $3/2^-[521]$ or $5/2^-[523]$, is involved in the structure of band C.

D. Band C of ^{162}Lu and bands D of ^{162,164}Lu

For band C of ^{162}Lu and band D of ^{164}Lu only one signature sequence is observed. In analogy to ^{166}Lu these bands probably correspond to the favored signature of the $\pi 1/2^-[541]\otimes\nu i_{13/2}$. No spin assignment has been made for ^{164}Lu, while in ^{162}Lu the I_0 value (see Fig. 5) lies between 9 and 12. Band D in ^{162}Lu is probably a four-quasiparticle band.

IV. ELECTROMAGNETIC PROPERTIES

From the experimental data the reduced transition probabilities can be determined by the expression

$$\frac{B(M1,I\rightarrow I-1)}{B(E2,I\rightarrow I-2)}=0.697\frac{E_{\gamma 2}^5}{E_{\gamma 1}^3}\frac{1}{\lambda(1+\delta^2)}\left[\frac{\mu_N^2}{(e\text{b})^2}\right],$$

where $E_{\gamma 1,\gamma 2}$ are the energies in MeV corresponding to the $\Delta I=1,2$ transitions, respectively, λ the γ-ray intensity ratio $I(\gamma_2)/I(\gamma_1)$, and δ the mixing ratio. The theoretical estimates of the $B(M1,I\rightarrow I-1)/B(E2,I\rightarrow I-2)$ were obtained using the semiclassical formula of the cranked shell model developed by Dönau and Frauendorf [58] (see also Ref. [1]). We used the expressions

$$B(E2,I\rightarrow I-2)=\frac{5}{16\pi}\langle IK20|I-2K\rangle^2 Q_0^2$$

and

$$B(M1,I\rightarrow I-1)=\frac{3}{8\pi}[(g_{\Omega_p}-g_R)(\Omega_p\sqrt{1-K^2/I^2}-i_pK/I)$$
$$+(g_{\Omega_n}-g_R)(\Omega_n\sqrt{1-K^2/I^2}-i_nK/I)]^2,$$

in units of μ_N^2. Q_0 is the intrinsic quadrupole moment, g_{Ω_p}, g_{Ω_n}, and $g_R=0.3$ are the proton, neutron, and collective gyromagnetic factors, respectively. The quantities i_p and i_n representing the aligned angular momentum of the proton and the neutron, respectively, were determined from the experimental data of the neighboring odd mass nuclei ^{161}Lu and ^{161}Yb for ^{162}Lu and ^{163}Lu and ^{163}Yb for ^{164}Lu. The g factors g_{Ω_p} and g_{Ω_n} were calculated by the expression [59]

$$g_\Omega=g_l+(g_s-g_l)\langle s_3\rangle/\Omega.$$

The expectation value of the spin projection on the symmetry axis $\langle s_3 \rangle$ was evaluated using Nilsson-type wave functions obtained from the diagonalization of the deformed harmonic oscillator with $\beta = 0.210$ for ^{162}Lu and $\beta = 0.233$ for ^{164}Lu and the parameters κ and μ were extracted from Ref. [59]. For the orbital and spin g factors we used $g_{l,p} = 1$, $g_{s,p} = 3.91$, $g_{l,n} = 0$, and $g_{s,n} = -2.68$. For ^{162}Lu (^{164}Lu) the adopted $Q_0 = 5.0(5.6)eb$ corresponds to the average over the quadrupole moments of the neighboring even-even nuclei. The $B(E2,2 \rightarrow 0)$ values extracted from the experimental lifetimes of neighboring even-even nuclei were used to obtain the quadrupole moments. Alignments and g factors for the proton and neutron intrinsic states used in the calculations are listed in Table IV. The moments of inertia and alignments were first roughly fitted from a cranking analysis from the experimental $\Delta I = 2$ transitions energies. The obtained values were subsequently used as a starting point for a more accurate calculation minimizing the difference between the experimental transitions and those expected from the VMI model. The theoretical estimates of the $B(M1)/B(E2)$ ratios obtained with this method for the possible configurations of the rotational bands were used to reproduce the experimental $B(M1)/B(E2)$ values below the band crossing (Figs. 11 and 17). The mixing ratio δ was evaluated from the expression

$$|\delta| = 0.832 E_\gamma(\Delta I = 1) \sqrt{B(E2, I \rightarrow I-1)/B(M1, I \rightarrow I-1)},$$

where $E_\gamma(\Delta I = 1)$ is the transition energy in MeV and the ratio $B(E2)/B(M1)$ is in units of $(eb)^2/\mu_N^2$. For most of the configurations the δ value was negligible and hence not taken into account. Only for the configuration $\pi 7/2^+[404] \otimes \nu i_{13/2}$ mentioned in the discussion of band C of ^{164}Lu the mixing ratio was appreciable and in this case $B(M1)/B(E2)(1+\delta^2)$ values were plotted (Fig. 17).

V. SUMMARY AND CONCLUSIONS

High-spin level schemes have been obtained for ^{162}Lu and ^{164}Lu comprising several rotational sequences. The bands have been identified on the basis of the coupling systematics for doubly odd nuclei belonging to the rare-earth region. For this purpose alignments, crossing frequencies, and $B(M1)/B(E2)$ ratios have been extracted and analyzed in the framework of the cranking model. The level staggering and signature inversion have been reviewed. The systematic behavior of signature-related oscillations in the yrast bands cannot be understood in the framework of the signature-dependent component of the Coriolis interaction.

Note added: At the time this work was being sent for publication, an article by the same principal investigators of Ref. [17] was just published reporting a complete study of ^{164}Lu [19].

[1] D. Hojman, A. J. Kreiner, M. Davidson, M. Debray, E. W. Cybulska, P. Pascholati, and W. A. Seale, Phys. Rev. C **45**, 90 (1992).

[2] A. J. Kreiner *et al.* (unpublished).

[3] G. Levinton, M. A. Cardona, M. E. Debray, D. Hojman, A. J. Kreiner, H. Somacal, J. Davidson, M. Davidson, D. De Acuña, D. R. Napoli, R. Burch, D. Bazzacco, N. Medina, S. M. Lenzi, C. Rossi Alvarez, N. Blasi, and G. Lo Bianco, Laboratori Nazionali di Legnaro–INFN(Rep) Annual Report No. 105/96, 1995 (unpublished), p. 74.

[4] Balraj Singh, Nucl. Data Sheets **75**, 199 (1995); G. Lo Bianco *et al.* (unpublished).

[5] A. Bruder, S. Drisi, V. A. Ionescu, J. Kern, and J. P. Vorlet, Nucl. Phys. **A474**, 518 (1987).

[6] A. J. Kreiner, Nucl. Phys. **A520**, 225c (1990).

[7] A. J. Kreiner and M. A. J. Mariscotti, Phys. Rev. Lett. **43**, 1150 (1979).

[8] A. J. Kreiner and M. A. J. Mariscotti, J. Phys. G **6**, L13 (1980).

[9] T. Komatsubara, K. Furuno, T. Hosoda, J. Mukai, T. Hayakawa, T. Morikawa, Y. Iwata, N. Kato, J. Espino, J. Gascon, N. Gjørup, G. B. Hagemann, H. J. Jensen, D. Jerrestam, J. Nyberg, G. Sletten, B. Cederwall, and P. O. Tjøm, Nucl. Phys. **A557**, 419c (1993).

[10] J. A. Pinston, S. André, D. Barnéoud, C. Foin, and J. Genevey, Phys. Lett. **137B**, 47 (1984), and references therein.

[11] S. Drissi, A. Bruder, J.-Cl. Dousse, V. Ionescu, J. Kern, J.-A. Pinston, S. André, D. Barnéoud, J. Genevey, and H. Frisk, Nucl. Phys. **A451**, 313 (1986).

[12] U. J. Schrewe, E. Hagberg, H. Schmeing, J. C. Hardy, V. T. Koslowsky, K. S. Sharma, and E. T. H. Clifford, Phys. Rev. C **25**, 3091 (1982).

[13] T. Hild, W.-D. Schmidt-Ott, V. Freystein, F. Meissner, E. Runte, H. Salewski, and R. Michaelsen, Nucl. Phys. **A492**, 237 (1989).

[14] M. A. Cardona, M. E. Debray, D. Hojman, A. J. Kreiner, H. Somacal, J. Davidson, M. Davidson, D. De Acuña, D. R. Napoli, J. Rico, D. Bazzacco, R. Burch, S. M. Lenzi, C. Rossi Alvarez, N. Blasi, and G. Lo Bianco, Z. Phys. A **354**, 5 (1996).

[15] P. Juneja, S. L. Gupta, S. C. Pancholi, Ashok Kumar, S. Muralithar, G. Rodrigues, R. P. Singh, and R. K. Bhowmik, Nuclear Science Centre, New Delhi, Annual Report No. 110067, 1992 (unpublished).

[16] S.-G. Zhou, Y.-Z. Liu, Y.-J. Ma, and C.-X. Yang, J. Phys. G **22**, 415 (1996).

[17] X.-H. Wang, C.-H. Yu, D. M. Cullen, M. Devlin, R. W. Ibbotson, M. R. Satteson, M. Simon, C. Y. Wu, D. C. Brian, D. M. Herrick, and K. Kurtz, Nuclear Structure Research Laboratory, Rochester, Annual Report 1993 (unpublished).

[18] P. Juneja, S. L. Gupta, S. C. Pancholi, Ashok Kumar, D. Mehta, L. Chaturvedi, S. K. Katoch, S. Malik, G. Shanker, R. K. Bhowmik, S. Muralithar, G. Rodrigues, and R. P. Singh, Phys. Rev. C **53**, 1221 (1996).

[19] X.-H. Wang, C.-H. Yu, D. M. Cullen, D. C. Bryan, M. Devlin, M. J. Fitch, A. Galindo-Uribarri, R. W. Gray, D. M. Herrick, R. W. Ibbotson, K. L. Kurz, S. Mullins, S. Pilotte, D. C. Radford, M. R. Satteson, M. W. Simon, D. Ward, C. Y. Wu, and L. H. Yao, Nucl. Phys. **A608**, 77 (1996).

[20] D. Bazzacco, in *Proceedings of the International Conference*

on Nuclear Structure at High Angular Momentum, Ottawa, 1992 [Report No. AECL 10613 (unpublished)], Vol. 2, p. 376.
[21] C.-H. Yu, M. A. Riley, J. D. Garrett, G. B. Hagemann, J. Simpson, P. D. Forsyth, A. R. Mokhtar, J. D. Morrison, B. M. Nyakó, J. F. Sharpey-Schafer, and R. Wyss, Nucl. Phys. **A489**, 477 (1988).
[22] W. Schmitz, C. X. Yang, H. Hübel, A. P. Byrne, R. Müsseler, N. Singh, K. H. Maier, A. Kuhnert, and R. Wyss, Nucl. Phys. **A539**, 112 (1992).
[23] S. Jónsson, J. Lyttkens, L. Carlén, N. Roy, H. Ryde, W. Waluś, J. Kownacki, G. B. Hagemann, B. Herskind, J. D. Garrett, and P. O. Tjøm, Nucl. Phys. **A422**, 397 (1984).
[24] P. Frandsen, R. Chapman, J. D. Garrett, G. B. Hagemann, B. Herskind, C.-H. Yu, K. Schiffer, D. Clarke, F. Khazaie, J. C. Lisle, J. N. Mo, L. Carlén, P. Ekström, and H. Ryde, Nucl. Phys. **A489**, 508 (1989).
[25] E. N. Shurshikov and N. V. Timofeeva, Nucl. Data Sheets **65**, 365 (1992).
[26] A. J. Kreiner, J. Davidson, M. Davidson, D. Abriola, C. Pomar, and P. Thieberger, Phys. Rev. C **36**, 2309 (1987); **37**, 1338 (1988).
[27] A. J. Kreiner, in *Proceedings of the International Conference on Contemporary Topics in Nuclear Structure Physics*, Cocoyoc, Mexico, 1988, edited by R. F. Casten, A. Frank, M. Moshinsky, and S. Pittel (World-Scientific, Singapore, 1988), p. 521, and references therein.
[28] A. J. Kreiner, in *Proceedings of the XII Workshop on Nuclear Physics*, Cataratas del Iguazú, Argentina, 1989, edited by M. C. Cambiaggio, A. J. Kreiner, and E. Ventura (World-Scientific, Singapore, 1989), p. 137.
[29] W. Schmitz, H. Hübel, C. X. Yang, G. Baldsiefen, U. Birkental, G. Fröhlingsdorf, D. Mehta, R. Mußler, M. Neffgen, P. Willsau, J. Gascon, G.B. Hagemann, A. Maj, D. Müller, J. Nyberg, M. Piiparinen, A. Virtanen, and R. Wyss, Phys. Lett. B **303**, 230 (1993).
[30] T. W. Burrows, Nucl. Data Sheets **56**, 313 (1989).
[31] D. Barnéoud and C. Foin, Nucl. Phys. **A287**, 77 (1977).
[32] C. Foin, D. Barnéoud, S. A. Hjorth, and R. Bethoux, Nucl. Phys. **A199**, 129 (1973).
[33] R. G. Helmer, Nucl. Data Sheets **59**, 1 (1990).
[34] J. Kownacki, J. D. Garret, J. J. Gaardhøje, G. B. Hagemann, B. Herskind, S. Jónsson, N. Roy, H. Ryde, and W. Waluś, Nucl. Phys. **A394**, 269 (1983).
[35] L. K. Peker, Nucl. Data Sheets **50**, 137 (1987).
[36] V. S. Shirley, Nucl. Data Sheets **58**, 871 (1989).
[37] M. S. Rosenthal, Diss. Abst. Int. **44B**, 216 (1983).
[38] J. C. Waddington, N. Lasheen, Y. Liang, and A. J. Larabee, McMaster University Annual Report, 1983 (unpublished), p. 73.
[39] S. Rastikerdar, C. Garret, and W. Gelletly, *Proceedings of the International Conference on Nuclei Far from Stability*, Helsinger, Denmark, 1981 (unpublished), Vol. II, p. 608; Report No. CERN-81-09, 1981 (unpublished).
[40] C. J. Gallagher, Jr. and S. A. Moszkowski, Phys. Rev. **111**, 1282 (1958).
[41] A. J. Kreiner, Phys. Rev. C **22**, 2570 (1980), and references therein.
[42] H. Sun, Y. Ma, H. Zheng, J. Zhang, Y. Ma, Y. Liu, C. Yang, S. Wen, G. Yuan, and G. Li, Z. Phys. A **351**, 241 (1995).
[43] S. Drissi, Ziping Li, M. Délèze, J. Kern, and J. P. Vorlet, Nucl. Phys. **A600**, 63 (1996).
[44] A. J. Kreiner, D. E. DiGregorio, A. J. Fendrik, J. Davidson, and M. Davidson, Phys. Rev. C **29**, R1572 (1984); Nucl. Phys. **A432**, 451 (1985).
[45] E. der Mateosian, Nucl. Data Sheets **48**, 345 (1986).
[46] L. K. Peker, Nucl. Data Sheets **58**, 93 (1989).
[47] R. G. Helmer, Nucl. Data Sheets **69**, 507 (1993).
[48] R. G. Helmer, Nucl. Data Sheets **65**, 65 (1992).
[49] R. G. Helmer, Nucl. Data Sheets **77**, 471 (1996).
[50] C. W. Reich, Nucl. Data Sheets **78**, 547 (1996).
[51] R. G. Helmer, Nucl. Data Sheets **64**, 79 (1991).
[52] E. N. Shurshikov and N. V. Timofeeva, Nucl. Data Sheets **67**, 45 (1992).
[53] V. S. Shirley, Nucl. Data Sheets **53**, 223 (1988).
[54] J. L. Salicio, M. Délèze, S. Drissi, J. Kern, S. J. Mannanal, and J. P. Vorlet, Nucl. Phys. **A512**, 109 (1990).
[55] S. J. Mannanal, B. Boschung, M. W. Carlen, J.-Cl. Dousse, S. Drissi, P. E. Garrett, J. Kern, B. Perny, Ch. Rhême, J. P. Vorlet, C. Günthe, J. Manns, and U. Müller, Nucl. Phys. **A582**, 141 (1995).
[56] R. G. Helmer, Nucl. Data Sheets **59**, 1 (1990).
[57] J. N. Mo, S. Sergiwa, R. Chapman, J. C. Lisle, E. Paul, J. C. Willmott, J. Hattula, M. Jääskeläinen, J. Simpson, P. M. Walker, J. D. Garrett, G. B. Hagemann, B. Herskind, M. A. Riley, and G. Sletten, Nucl. Phys. **A472**, 295 (1987).
[58] F. Dönau and S. Frauendorf, in *Proceedings of the Conference on High Angular Momentum Properties of Nuclei*, Oak Ridge, Tennessee, 1982, edited by N. Johnson (Harwood Academic, Chur, Switzerland, 1982), p. 143.
[59] A. Bohr and B. Mottelson, in *Nuclear Structure* (Benjamin, Reading, MA, 1975), Vol. 2.